Journal of Physics:
Conference Series

PURPOSE-LED
PUBLISHING™

PAPER • OPEN ACCESS

# A High-Resolution WRF Case Study of a Thunderstorm-Induced Cold Pool and Impacts on Wind Turbine Power Output, Wake Structure and Mechanical Loading

To cite this article: Gerard Kilroy *et al* 2026 *J. Phys.: Conf. Ser.* **3224** 022062

View the article online for updates and enhancements.

You may also like

- On the robust autorotation of a samara-inspired rotor in gusty environments
  Adnan M El Makdah, Kai Zhang and David E Rival
- Shoulder viscoelasticity in a raptor-inspired model alleviates instability and enhances passive gust rejection
  Samuel C Stanton
- Effect of cooling roofs on gust wind speed over an urban agglomeration in Southern China
  Xueyuan Wang, Gang Liu, Hongnian Liu et al.

This content was downloaded from IP address 129.247.247.239 on 28/05/2026 at 16:17

The Science of Making Torque from Wind (TORQUE 2026) IOP Publishing
Journal of Physics: Conference Series **3224** (2026) 022062 doi:10.1088/1742-6596/3224/2/022062

# A High-Resolution WRF Case Study of a Thunderstorm-Induced Cold Pool and Impacts on Wind Turbine Power Output, Wake Structure and Mechanical Loading

**Gerard Kilroy**[1], **Jeffrey D. Thayer**[1], **Julia Menken**[1], **Oliver Hach**[2] and **Felix Krimm**[2]

[1]Institute of Atmospheric Physics, German Aerospace Center (DLR), Oberpfaffenhofen, Germany

[2]Institute of Aeroelasticity, German Aerospace Center (DLR), Göttingen, Germany

E-mail: gerard.kilroy@dlr.de

**Abstract.** Convective cold-pool gust fronts represent extreme inflow conditions for wind-energy systems, yet their impacts on turbine wakes and loading remain poorly quantified. This study presents a high-resolution numerical case study of a strong cold-pool gust front simulated with the WRF model coupled to a generalized actuator disk representation of a wind turbine. The event is characterized by three distinct atmospheric-boundary-layer regimes: a marginally convective pre-gust boundary layer, a highly turbulent gust-front passage, and a strongly stabilized post-gust period.

During the gust front, hub-height wind speeds more than double relative to pre-gust conditions, reaching values close to 24 $\mathrm{m\,s^{-1}}$. This wind ramp is accompanied by rapid wind direction changes and a near-surface temperature drop of approximately 6 K. The enhanced turbulence during the gust-front passage substantially reduces the turbine wake velocity deficit and accelerates wake recovery, while the stabilized post-gust environment leads to a stronger and more persistent wake. Changes in rotor-layer shear and veer during the event would have important implications for wake structure. The analysis of out-of-plane blade root bending moments indicates that mechanical loading responds primarily to changes in turbine operating regime rather than directly to variations in wind shear associated with the gust-front passage. These results highlight the importance of convective cold-pool dynamics for wind-turbine performance and wake behavior.

## 1. Introduction

Deep convective clouds (or thunderstorms) are associated with a range of high-impact atmospheric processes, including electrification and lightning, hail formation, rapid reductions in solar irradiance, intense precipitation, and abrupt variations in wind speed and direction (wind ramps). General overviews of deep convective clouds including the dynamical processes involved are given in Chapter 8 of Wallace and Hobbs [1] and in Chapters 7-8 of Houze [2]. These phenomena are particularly difficult to forecast due in part to their intrinsically stochastic nature

Content from this work may be used under the terms of the Creative Commons Attribution 4.0 licence. Any further distribution of this work must maintain attribution to the author(s) and the title of the work, journal citation and DOI.
Published under licence by IOP Publishing Ltd

and their relatively short life times, with the majority of convective cells decaying in under one hour [3]. The rapid changes in wind speed and direction associated with thunderstorm outflow near the surface (also known as cold-pool gust fronts) have an impact on wind energy applications. These gust fronts not only affect power output, but also stress turbine blades due to increased mechanical loads on the wind turbines [4].

Recent observational work by Thayer *et al.*, (2025) [5] quantified the effects of cold-pool passages over the WiValdi research wind park[1] in northern Germany in the context of wind energy. The authors detected 120 convective cold pool passages over a period of 4 years and showed a median hub-height wind speed perturbation during gust front passage of about 4 m $s^{-1}$, with an associated relative wind direction shift up to 15°. In particular, they showed that there is an increase in estimated power of up to 50% during the median cold-pool passage, with increased power output lasting around 30 minutes. To further quantify the possible effects of cold-pool gust fronts for wind energy applications over Germany, Kilroy and Thayer (2025) [6] performed a month-long Weather Research and Forecasting (WRF) simulation for July 2023. Following a Lagrangian approach, they showed that throughout the typical thunderstorm life cycle, estimated power output increases from 33-60%.

While deep-convective cold pools are relatively short-lived events, and occur relatively infrequently - between 24 and 44 times per summer season (as seen in observational data near Hamburg [7]), it is nevertheless important to quantify their effects for minute-scale wind-power forecasting in the energy trading sector, as the German electrical grid currently operates on lead times down to 5 minutes [8]. The typical cold-pool gust front would likely impact many turbines or wind parks simultaneously, considering the median observed cold-pool has an associated parent deep-convective cell size of about 225 $km^2$ [6].

Convective gust fronts are not only associated with temporarily increased wind speeds, but following the passage of the gust, there are reduced winds and a temporary stabilization of the boundary layer. Changes in near-surface thermal stability within the atmospheric boundary layer (ABL), such as those caused by cold-pool passages, also influence wind turbine power generation. Convective boundary layers promote stronger turbulence and faster wake recovery, while stable boundary layers suppress turbulence and prolong wake effects [9, 10]. During cold-pool passage, there is additional complexity. Gust fronts enhance turbulence briefly during passage [5], whereas the cold-pool interior increases near-surface stability [5, 6, 11]. The boundary-layer stabilization lasts up to two hours [12] and impacts the structure and duration of the turbulent wake produced by the turbine.

Previous work has quantified the effects of larger-scale meteorological phenomena, such as a mesoscale frontal passage, in simulations of a utility-scale wind farm [13] using a generalized actuator disk (GAD) parameterization, showing good agreement with observations. Others capture evolving ABL characteristics and wake effects over a longer time period in large eddy simulations (LES) of a diurnal cycle [14, 15]. While the effects of an idealized thunderstorm downburst (a particularly strong convective downdraft) in model output has been studied in terms of loads generated on a turbine [16], as far as we are aware, there has been little research into cold-pool passages over wind turbines and the impacts of the short-term atmospheric stability changes on turbine wakes (on timescales shorter than one hour).

In this work, we use the WRF-LES-GAD framework to perform a case study of a particularly strong simulated cold-pool passage over the location of the WiValdi wind park during the month of July 2023. The main aim is to gain a more complete understanding of the behavior of the

---

[1] More information about the wind park can be found on the official website (https://www.windenergy-researchfarm.com).

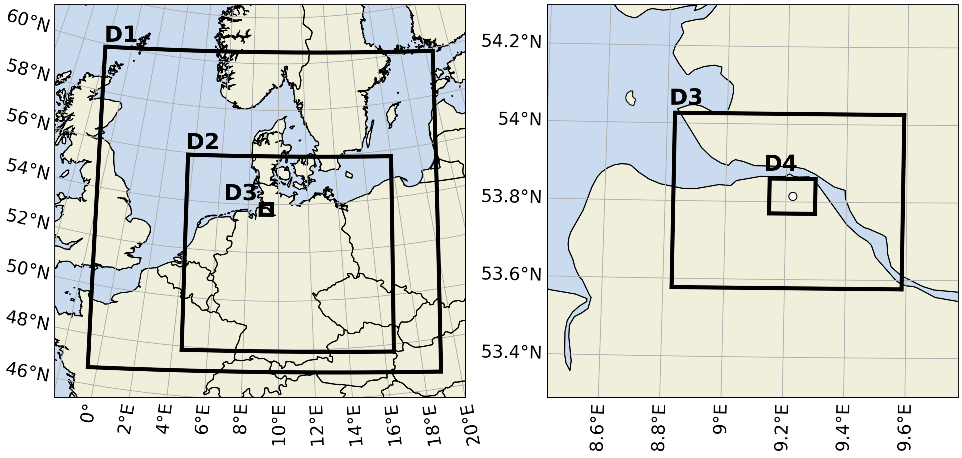

**Figure 1.** Domain setup for the WRF simulation. The right panel focuses on the innermost domains. The location of the WiValdi wind park is shown by a white dot in the right panel.

turbine wake produced during the cold-pool passage, in terms of the wake deficit and structure during the rapidly-changing atmospheric conditions. We want to determine how long it takes for the wake to recover to its pre-environment structure and aim to quantify the changes in power output from the turbines. An additional aim is to quantify the structural loads experienced from a cold-pool passage on a turbine using a commercial turbine simulation tool.

## 2. Methodology

The simulation presented herein is performed using WRF (V4.4.1), a state-of-the-art, non-hydrostatic model widely utilized in the meteorological community for both operational forecasting and research purposes [17]. WRF solves the fully compressible Euler equations, employing a terrain-following, hybrid sigma-pressure vertical coordinate system. The numerical model configuration is as presented in Kilroy and Thayer (2025) [6], with an extension of two additional inner LES domains. Here, there are four nested domains with horizontal grid spacings of 5 km, 1 km, 100 m and 20 m. The innermost domain, Domain 4 (D4), which is the focus of this study, has 91 vertical levels (6 of those are located within the typical rotor layer - for the turbines located at WiValdi this would cover the height range from 34 to 150 m above ground level; see below for information on the turbine parametrization). Initial and boundary conditions are supplied from the European Centre for Medium-Range Weather Forecasts (ECMWF) operational analyses, provided every 6 hours.

For all domains, the three-dimensional turbulent kinetic energy subgrid mixing scheme that is self-adaptive to the grid size between the large-eddy simulation and mesoscale scales is utilized [18]. The WDM 6-class microphysics scheme [19] is used in all inner domains. The domain setup is displayed in Figure 1. While the outer two domains are simulated for the entire month of July 2023, the innermost two domains are initiated just over half-way through the month, immediately prior to a particularly strong cold-pool event which occurred at the location of the WiValdi wind park (highlighted in Fig. 1). D3 is initiated at 0600 UTC 15 July, and D4 is initiated 6 hours later. The cold pool itself impacted the wind park location at roughly 1330 UTC 15 July. For the two-hour period from 1300 - 1500 UTC, model output is produced every 1 minute. The wind turbine parametrization is implemented in WRF with the blade-element momentum theory [20],

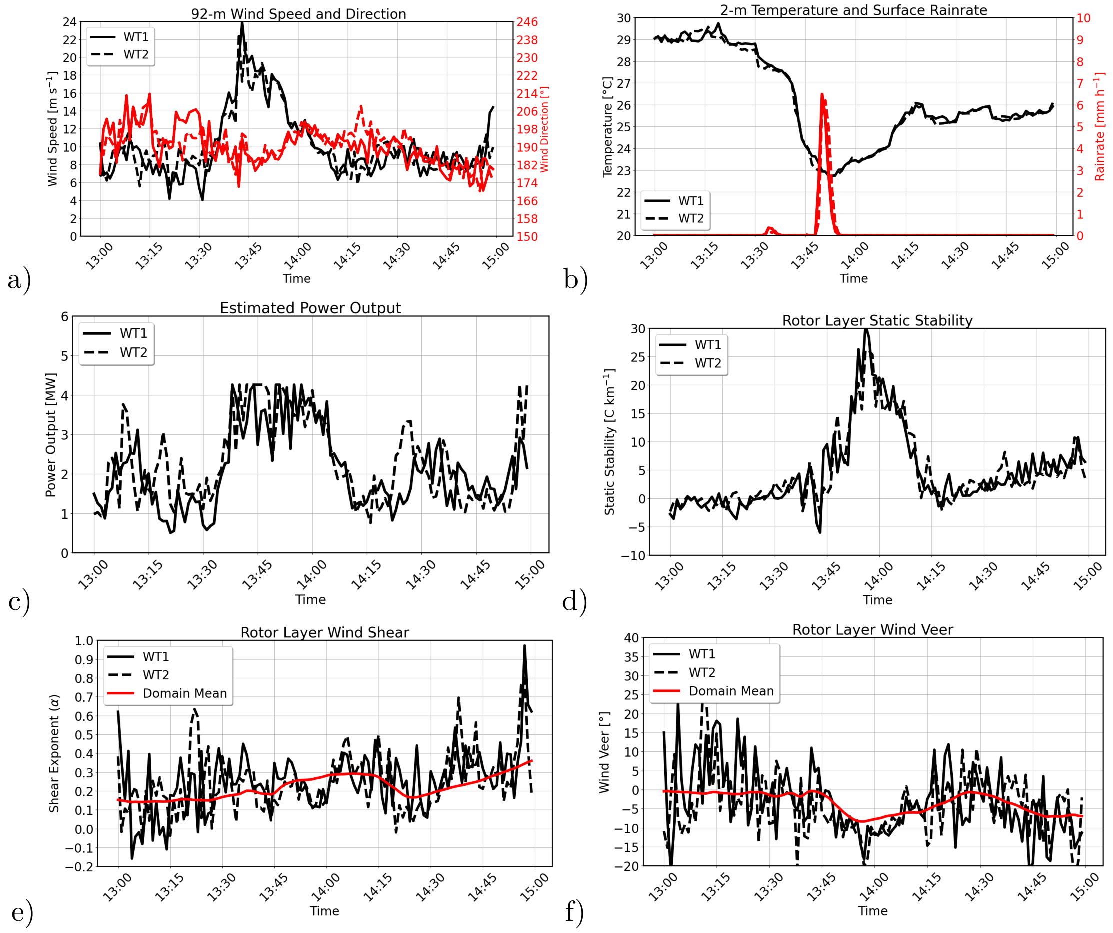

**Figure 2.** Time series of (a) 92-m wind speed (m s$^{-1}$) and direction (°) (b) 2-m temperature (°C) and rain rate (mm h$^{-1}$), (c) estimated power output (MW), (d) rotor-layer static stability (C km$^{-1}$), (e) rotor-layer shear exponent $\alpha$ and (f) rotor-layer veer (°) for the first (WT1) and second (WT2) turbine for the 2-hour simulation period. Shown also in panels (e-f) are the domain mean quantities (solid red curves).

where the thrust and rotational (torque) forces are calculated from the inflow wind field, and are averaged over a discretized two-dimensional disk and applied to the momentum equations in the vicinity of the turbine location. The turbines are able to yaw into the oncoming wind. Two turbines are defined by the National Renewable Energy Laboratory (NREL) 5-MW reference wind turbine, with hub heights (92 m) and rotor diameters chosen (D = 116 m) to match those of the Enercon E-115 EP3 4.3 MW turbines installed at the WiValdi wind park. While the choice of 20-m horizontal grid spacing is relatively coarse and corresponds to roughly 6 grid points covering the rotor region of the implemented turbine, several studies have found that it is sufficient for capturing the broad-scale wake features within the turbine operating area [21–23]. Additionally, the so-called cell perturbation method (CPM) [24] is included in all LES domains to accelerate the development of realistic small-scale turbulence. The implementation of CPM in WRF has been shown to produce much more realistic turbulent fields at the WiValdi wind park, when compared to LES simulations without [25].

In order to calculate the blade root bending moments for the turbine blades, the commercial turbine simulation tool Bladed (version 4.11, [26]) is utilized. It employs a multibody model of

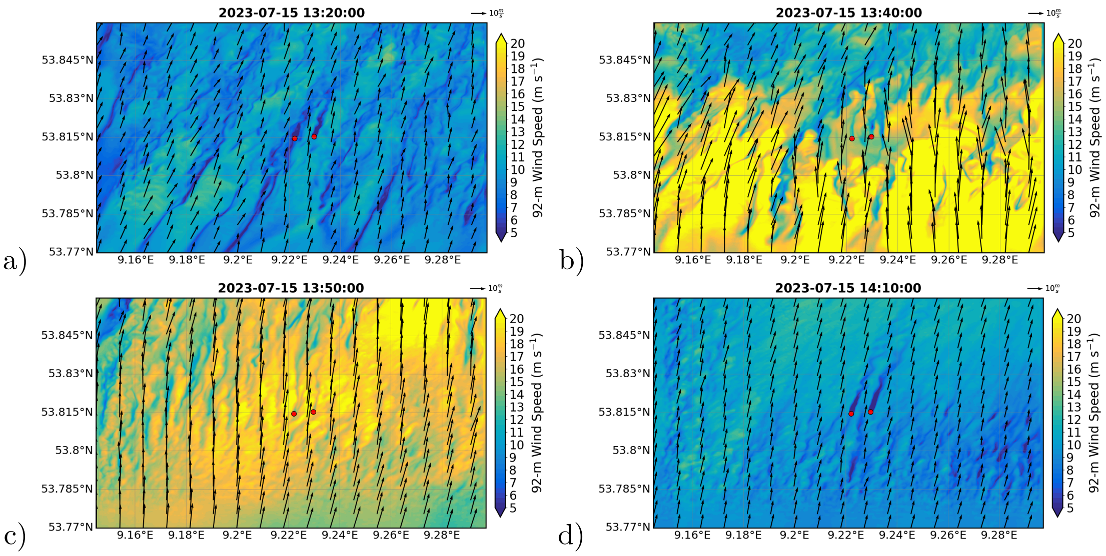

**Figure 3.** Instantaneous horizontal cross sections of 92-m wind speed for a) 1320 UTC, b) 1340 UTC, c) 1350 UTC and d) 1410 UTC, times covering the entire cold-pool passage, with the peak wind gust occurring at 1343 UTC. Wind vectors (m s$^{-1}$) at a height of 92 m are shown, with the reference vector given in the upper right of each panel. Highlighted are the locations of the two parametrized turbines (red dots).

the Enercon E-115 EP3 turbine, including tower and blade flexibility as linear elastic bodies, and a BEM type aerodynamic model. The environmental conditions for the simulations are input through a wind field file (full-field Bladed convention) that is generated from the WRF simulation output, extracted in a plane 320 m upstream of the turbine. Only the relevant section of each of these slices is used, resulting in a wind field on a 140 m x 140 m grid in lateral and vertical direction, centered around the rotor hub. This conversion must be regarded as an approximation, since the longitudinal offset cannot be incorporated into the Bladed simulation, so that extracted wind velocities are applied directly in the rotor plane. Additionally, smaller-scale turbulent structures are not captured in the wind field due to the 1-minute sampling time. In total, five 15-minute load simulations are carried out to cover the range from 1315 - 1430 UTC, and to assess blade load variations in the different atmospheric regimes before, during, and after the gust. The simulation model incorporates a turbine controller - responsible for pitch, torque, and yaw regulation - ensuring that variations in wind conditions induce realistic changes in the operating point.

## 3. Results

In the following, the analysis of this test-case cold-pool impact is split into three distinct sections. First, the atmospheric inflow environment, defined as the location 2D upstream of the turbines, is investigated. This location upstream was chosen to avoid including in the analysis the effects of the turbine itself on the flow field, including blockage effects. Next, we analyze the horizontal structure of the wake produced by one of the turbines using a wake detection algorithm. Finally, we investigate the loads experienced by a turbine impacted by the cold-pool passage.

### *3.1. Inflow Fields*

Figure 2 shows time series of various quantities including the wind speed and direction at 92-m height, the 2-m temperature and surface rainrate and estimated power output for the two-hour time period from 1300 - 1500 UTC July 15. Additionally, the rotor-layer (34-150 m height above ground level) static stability, wind shear and veer are presented.

Initially, the wind speeds upstream of both turbines fluctuate between 6-10 m $s^{-1}$ until about 1330 UTC (Fig. 2a). At this time, the winds rapidly increase in strength to a peak of about 24 m $s^{-1}$ at 1343 UTC. Over the following 15-25 min, the wind speeds decrease back to their pre-ramp values. While the wind direction fluctuates strongly in the convective pre-cold-pool environment, there is a change of around 20° associated with the onset of the gust front itself. From about 1330 UTC, the temperature begins to decrease sharply (Fig. 2b), with a drop as large as 6° C occurring at 1350 UTC. At this time, relatively strong rainfall is recorded (over 6 mm $h^{-1}$). The associated power output calculated within the WRF-GAD framework[2] is shown in Figure 2c. Power output for both turbines peaks following the onset of the gust and remains close to maximum output (4.3 MW) for a time period of 20-25 minutes.

The rotor-layer static stability remains close to or just below zero up until 1330 UTC, indicating that the pre-gust environment is marginally convective (Fig. 2d). Following the onset of the gust, there is a sudden and dramatic regime change, with the environment becoming strongly stably stratified (reaching a peak of 30°C $km^{-1}$ at 1357 UTC). A recovery of the boundary layer to the pre-gust stratification occurs by 1415 UTC. The strongest stratification change occurs after the 92-m wind speed peak and surface cooling occur. This stabilization occurs as the cold, negatively buoyant air at the core of the cold pool passes over the wind park. The denser, cooler air is generated primarily through evaporative cooling of precipitation and the melting of ice hydrometeors both within the cloud and below cloud base.

The wind-shear exponent $\alpha$, a dimensionless parameter that characterizes the vertical variation of wind speed with height, increases throughout the domain from $\alpha = 0.15$ prior to gust impact to a peak of $\alpha = 0.3$ between 1400-1415 UTC (Fig. 2e). Interestingly, this peak wind shear in the domain occurs after the wind speed peak has occurred, during a time period when the wind speeds are returning to pre-gust environment values. There are large fluctuations at the locations upstream of both turbines throughout the simulation. Similarly, there are large variations in the rotor-layer wind veer (Fig. 2e). In a domain-mean sense, however, the wind veer turns from close to zero to negative around the time the wind speeds peak. This counterclockwise turning of winds with height has been found in observations of cold pools at the WiValdi wind park [5], and is explained by greater wind direction changes occurring closer to the surface. Negative veer (counter-clockwise turning hodograph) is opposite to the typical northern-hemisphere climatological behavior for stable boundary layers, which typically is positive with height (clockwise turning hodograph, a canonical result of Ekman boundary-layer dynamics). Negative veer generated by the cold-pool passage, in combination with the strong stabilization, would impact the wake structure and the direction of the deflection [27].

Horizontal cross sections show the full domain flow fields at 92-m height (Fig. 3) for 1320, 1340, 1350 and at 1410 UTC, specific times that well capture the pre-cold pool environment (panel a), the onset and passage of the main gust component (panels b and c) and the stabilized environment with reduced winds after the gust passage (panel d). So-called lobe-and-cleft instabilities (which appear in simulations with grid spacing finer than approximately 100-m [28]) are evident along the leading edge of the cold-pool gust front as it passes through the domain (Fig. 3b). The turbulent flow associated with realistic cold pools appears to be well captured in this simulation. By 1410 UTC, the wind speeds have returned to initial values, however the

---

[2] In the GAD code implemented in WRF, turbine power output is estimated from the work done on the flow by rotor forces. The local tangential forces resolved over the actuator disk are integrated over grid cells intersecting the rotor to compute the total power extracted, consistent with the generalized actuator disk theory.

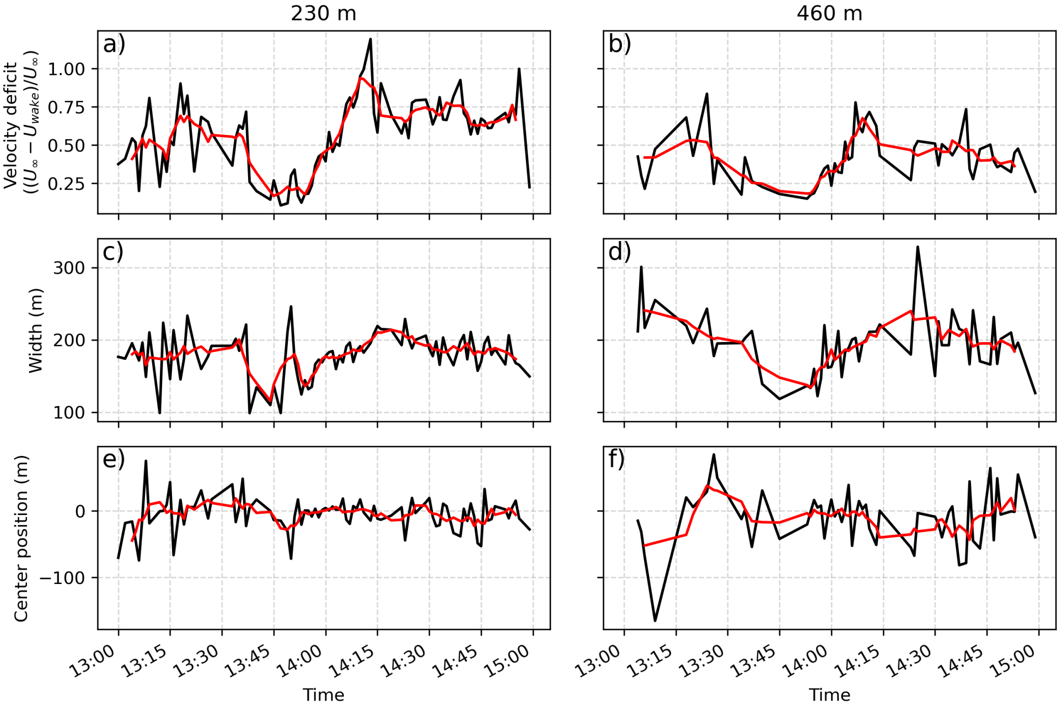

**Figure 4.** Time series of 92-m velocity deficit (a, b), wake width (m) (c, d), and the wake center position (m) (e, f) at distance downstream of 2D (a, c, e) and 4D (b, d, f) from the first wind turbine (WT1). The black lines represent the timeseries, while the red lines show the 5-minute rolling mean for the 2-hour simulation.

boundary-layer stratification at this time is strongly stable. This is evident in both the appearance of smaller-scale turbulence and the more distinguished turbine wakes behind both turbines (as characterized by both wake deficit and length). An analysis of wake structure is the topic of the next subsection.

### *3.2. Wake Structure*

In this section, we utilize a wake detection algorithm [29] in order to better understand how turbine wakes are affected by the passage of a convective cold-pool. We focus this wake analysis on the wake produced by the first turbine, WT1. The wake detection algorithm applies Gaussian fits to the velocity field behind WT1 in order to extract wake amplitude, width and center point. In particular, the turbine wake boundaries are identified throughout the cold-pool passage in order to quantify the atmospheric effects on wake structure and recovery. In Figure 4, we show time series of 92-m velocity deficit, wake width, and the wake center position at distances downstream of 2D and 4D. In Figure 5, we show also horizontal slices and cross sections of wake deficit at hub height. The right-handed coordinate system with x pointing downstream is aligned with the wind direction of the inflow 2D upstream of WT1, according to the wind direction at WT1. The inflow velocity $U_\infty$ is considered as the value 2D upstream.

Prior to the gust-front impact, the wake deficit at 2D downstream is typically between 0.5 and 0.75, with fluctuations occurring in the marginally convective boundary layer (Fig. 4). As the gust front passes over the turbine, there is a large and sudden drop in wake deficit with values around 0.25 or lower occurring for a roughly 20-minute period which coincides with

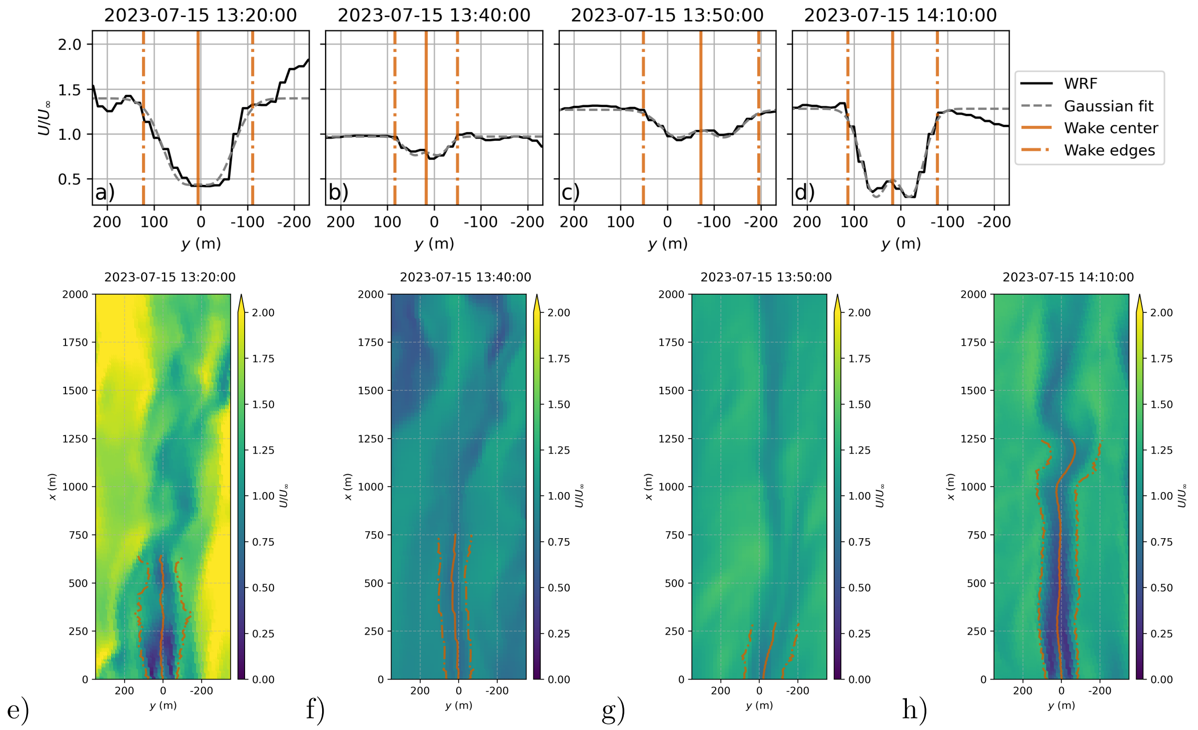

**Figure 5.** Horizontal slices of hub-height wake deficit at 2D downstream of WT1 (top row) and horizontal cross-sections of wake deficit at four instances throughout the time period of interest (bottom row). A Gaussian fit is shown in the upper panels and is used in order to extract amplitude, wake width and center point. In all panels the solid orange lines represent the centerline of the wake and the dash-dotted orange curves the horizontal width of the wake.

a brief increase in atmospheric instability around 1340 UTC. Meanwhile, the turbine reaches its rated power, the blades pitch, its power coefficient decreases, resulting in relatively less energy extracted from the wind, which corresponds to a reduced wake deficit and wake width. The reduction of the thrust force due to blade pitching is presumably the main reason for the significant reduction of the wake deficit. Additionally, in the stably-stratified boundary layer following the gust passage, the deficit is often larger than in the pre-gust environment as the turbulence strength decreases, the thrust coefficient increases due to reduced blade pitching and turbulent mixing of the wake is reduced. At 4D downstream of WT1, the situation is similar, however, the wake becomes more turbulent and meandering, making it more difficult to detect further downstream. The wake width also appears to decrease in size around the time of the gust-front passage, with a larger wake occurring in the stable regime (after 1400 UTC). The wake center position fluctuates around zero with larger perturbations further downstream. In idealized studies, a backing wind (or negative veer) tends to deflect the upper half of the wake to the left, and the lower half to the right, with hub height winds typically not undergoing any deflection downstream ([30]; see their Figure 9). The investigation of wake deflection at different heights in this gust case is worthy of further investigation.

Following from the analysis of D4 shown in Figure 3, we now provide a detailed examination of the turbine wake itself given in Figure 5, which highlights the horizontal structure at times covering the entire cold-pool passage. The top panel in this figure shows horizontal slices of relative wind velocities and center location at 2D downstream for these times. The solid lines represent the centerline of the wake and the dash-dotted curves the horizontal width of the wake. These curves disappear in the lower panels when the wake is no longer distinguishable from the surrounding atmospheric flow given the wake detection termination conditions, which occurs closer to a turbine in convective regimes. The wake deficit is more reduced in the time periods where the gust is over the turbines, 1340 and 1350 UTC, however, it is often difficult to detect further downstream. While the wake deficit is relatively large in the marginally-convective environment (1320 UTC), it's length is shorter than in the stably-stratified one (1410 UTC).

## 4. Mechanical Loads

Finally, in this subsection, we quantify the mechanical and structural loads experienced by a turbine impacted by an inflow-wind field associated with the cold-pool passage. Unlike the wake and power output calculations presented above, the mechanical loads shown below are not calculated in the WRF-GAD setup, but rather via extracted wind fields located 2D upstream of the modeled turbines in WRF that are then run through an additional load model, Bladed.

Figure 6 shows the resulting out-of-plane root bending moment of blade 1 in the hub coordinate system for the five individual simulation periods as polar plots over the rotor angle, normalized by the mean value of the first period. Each of the diagrams contains the time series of the bending moment as a light blue line, its average as a black line, and the average for a specific rotor angle as a dark blue line. A variation of the average bending moment manifests as the distance between the plotted lines and the diagram origin. Conversely, wind velocity gradients across the rotor plane (e.g., due to shear or veer) induce changes in the graphs' asymmetry. Comparing the periods with the wind speeds in Figure 2a reveals that the operating conditions are different between the simulations. Moving from left to right, an increase in the average bending moment is observed for the fourth period, where the wind speed is close to nominal conditions, as one would expect. In contrast, the average bending moments are lower in the second and third periods, where the turbine is operated at nominal power with nominal rotor speed and pitched blades. It is also observed that the azimuthal average is shifted to the right in each of the plots, representing an asymmetric distribution of the loading with respect to the rotor angle. The difference between these shifts appears to be marginal. A pronounced influence of variations of wind shear, shown in Fig. 2e, could not be found in the mechanical loads of the turbine.

Hannesdóttir *et al.*, (2019) [31] showed that ramp-like wind speed increases similar to those associated with cold pool gust fronts can produce transient increases in blade root flapwise and edgewise bending moments as wind speeds approach rated conditions while above rated wind speed the activation of blade pitch control moderates further load growth. While the referenced study examined the statistical influence of turbulent inflow on turbine loads, our analysis focuses on a single well-defined event; future work will extend this approach to a broader set of cases.

## 5. Conclusions

This work aims to quantify the impact of a particularly strong cold-pool gust front on wind-energy applications. We perform a high-resolution case study of a simulated gust front in order to better understand the changes in the inflow environment, the impacts on the turbulent wake produced by a turbine, and the changes in mechanical loads during a cold-pool gust front passage. The analysis shows three distinct regimes: a marginally-convective boundary layer before impact, the turbulent gust itself, and a period of stabilization following the gust passage.

The cold-pool gust front case analyzed herein leads to a more than doubling of the hub-height

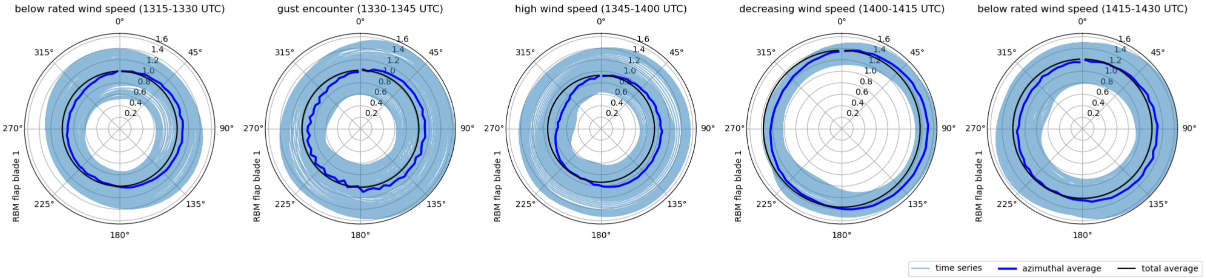

**Figure 6.** Normalized flapwise root bending moments of blade 1 from Bladed simulations in response to the gust passage (from 1315 - 1430 UTC).

background winds, with a peak close to 24 m $s^{-1}$ and an associated wind direction change of about 20°. A near-surface temperature drop of 6 ° C was found, with a recovery of only 3 ° C occurring within the 2-hour simulation. During the gust front passage, estimated power output reaches a maximum for a time period of 20-25 minutes. There is also a stark change in rotor-layer thermal stability, wind shear and veer both during and after passage, when compared to the marginally-convective pre-gust boundary layer. In general, wind shear nearly doubles in strength over the rotor layer as the boundary layer becomes strongly stabilized. There is a systematic change in wind veer throughout the domain, which becomes negative during the gust passage, opposite to typical northern-hemisphere climatological behavior. Changes in rotor-layer shear and veer during the event would have important implications for wake structure. Horizontal cross sections reveal also the turbulent nature of the gust front itself.

Analysis of the wake structure indicates that the cold-pool passage strongly modulates the turbine wake. In the marginally convective pre-gust environment, the wake deficit exhibits strong temporal variability. During the cold-pool gust front passage, due to the fact that turbine reaches rated power and due to enhanced turbulence dramatically reducing the wake velocity deficit, there is a smaller wake in terms of horizontal extent, indicating rapid wake recovery. In the stabilized period following the gust front, the wake deficit increases to values exceeding those observed prior to the gust, while the wake width returns to pre-gust levels, resulting in a longer and more persistent wake. These results highlight the contrasting impacts of turbulence enhancement during cold-pool passage and boundary-layer stabilization thereafter on wake strength and structure.

From the current load analysis, we do not find that this gust front passage induces critical structural stress on the simulated turbines within accompanying aeroelastic simulations. This is presumably due to the ability of the turbine control system to sufficiently react to the rapidly-changing environmental conditions. The resulting turbine operating conditions seem to have a much bigger impact on the structural loads than variations in the atmospheric inflow.

While a direct comparison between the simulated gust-front case and a specific observed event is not possible due to the stochastic nature of deep convection and the absence of a real-world counterpart at the exact simulation time, the choice of focusing the simulation around the WiValdi research wind park enables future statistical comparisons with observed convective gust fronts of comparable intensity. As the wind park was officially commissioned on 15 August 2023, after the period analyzed herein, forthcoming observations will allow for systematic comparison between modeled and observed bulk cold-pool characteristics. The observational infrastructure includes an upstream meteorological mast, vertically-profiling Doppler wind lidar, and a microwave radiometer for characterization of the inflow conditions throughout the rotor layer depth. In addition, a nacelle-mounted lidar on WT1 provides the opportunity to validate WRF–GAD wake simulations, while turbine-mounted sensors enable validation of the modeled structural loads. These comparisons will be the focus of future work.

## Acknowledgements

We are grateful to two anonymous reviewers for their thoughtful reviews of the original article. This work used resources of the Deutsches Klimarechenzentrum (DKRZ) granted by its Scientific Steering Committee (WLA) under project ID bd1069.

## References

[1] Wallace, JM, Hobbs PV, 2006. *Elsevier*, Amsterdam, **352-353, 357, 367-368.**
[2] Houze, RA, 2014. *International Geophysics* **(Vol. 104, 432 p.)**. Amsterdam: Academic Press.
[3] Wapler, K, 2021. *Atmospheric Research*, **248**, 105186.
[4] Kelly M, *et al.*, 2021. *Wind Energ. Sci.*, **6**, 1227–1245.
[5] Thayer, JD, *et al.*, 2025. *Wind Energ. Sci.*, **10**, 2237-2255.
[6] Kilroy, G, Thayer, JD, 2025. *QJRMS*, **e70042**, 2025.
[7] Kirsch S, *et al.*, 2021. *Monthly Weather Review*, **149**, 811–820.
[8] Würth, I, *et al.*, 2019. *Energies*, **12(4)**, 712.
[9] Stull, RB, 1988. *Atmospheric and Oceanographic Sciences Library*, Vol. **13**, Kluwer Academic, 670 pp.
[10] Zhang, W, *et al.*, 2013. *Boundary-Layer Meteorol*, **146(2)**:161–179.
[11] Canepa, F, *et al.*, 2020. *J. Wind Eng. Ind. Aerod.*, **206**, 10433.
[12] Kruse, IL, *et al.*, 2022: *QJRMS*, **148**, 711–726.
[13] Arthur, R.S., *et al.*, 2020. *Atmosphere*, **11(3)**, 245.
[14] Englberger A, Dörnbrack A, 2018. *Boundary-Layer Meteorology* **166**, 423-448.
[15] Vollmer L, *et al.*, 2017. *J. Phys.: Conf.* Ser. **854** 012050.
[16] Nguyen, HH, and Manuel, L, 2014. *Energies*, **7(10)**, 6527-6548.
[17] Skamarock WC, *et al.*, 2008. *NCAR technical note*, Mesoscale and Microscale Meteorology Division, National Center for Atmospheric Research, Boulder, Colorado, USA.
[18] Zhang X, *et al.*, 2018. *Mon. Wea. Rev.,* **146**, 2023–2045.
[19] Hong SY, Lim JOJ, 2006. *J. Korean Meteor. Soc.,* **42**, 129–151.
[20] Mirocha JD, *et al.*, 2014. *J. Renewable Sustainable Energy*; **6 (1)**.
[21] Pena, A, *et al.*, 2022. *Mon. Wea. Rev.,* **150**, 3051–3064.
[22] van der Laan, MP, *et al.*, 2023. *Wind Energ. Sci.*, **8**, 819–848.
[23] Bui, H, *et al*, 2024. *Geosci. Model Dev.*, **17**, 4447–4465.
[24] Muñoz-Esparza, *et al.*, 2014. *Boundary-Layer Meteorol* **153**, 409–440.
[25] Kilroy G, *et al.*, 2024 *J. Phys.: Conf. Ser.* **2767** 052063
[26] DNV-GL©, Bladed, Version 4.11: https://www.dnv.com/software/services/bladed/
[27] Englberger, A, Lundquist, J, 2020. *Journal of Physics: Conference Series*, **1452**.
[28] Fievet, R, *et al.*, 2023. *Journal of Advances in Modeling Earth Systems*, **15**.
[29] Menken J, *et al*, 2026. *Wind Energ. Sci.*, **submitted**.
[30] Englberger, A, *et al*, 2020. *Wind Energ. Sci.*, **5**, 1623–1644.
[31] Hannesdóttir, Á., *et al.*, 2019. *Wind Energ. Sci.*, **4**, 325–342.